batteries

MDPI

*Article*

# A Coordinated Control Strategy for Efficiency Improvement of Multistack Fuel Cell Systems in Electric–Hydrogen Hybrid Energy Storage System

**Jianlin Li, Ce Liang * and Zelin Shi**

National User-Side Energy Storage Innovation Research and Development Center, North China University of Technology, Beijing 100144, China; dkyljl@163.com (J.L.); szl835597416@126.com (Z.S.)
* Correspondence: lc1051574441@163.com

**Abstract:** A two-layer coordinated control strategy is proposed to solve the power allocation problem faced by electric–hydrogen hybrid energy storage systems (HESSs) when compensating for the fluctuating power of the DC microgrid. The upper-layer control strategy is the system-level control. Considering the energy storage margin of each energy storage system, fuzzy logic control (FLC) is used to make the initial power allocation between the battery energy storage system (BESS) and the multistack fuel cell system (MFCS). The lower-layer control strategy is the device-level control. Considering the individual differences and energy-storage margin differences of the single-stack fuel cell (FC) in an MFCS, FLC is used to make the initial power allocation of the FC. To improve the hydrogen-to-electricity conversion efficiency of the MFCS, a strategy for optimization by perturbation (OP) is used to adjust the power allocation of the FC. The output difference of the MFCS before and after the adjustment is compensated for by the BESS. The simulation and experiment results show that the mentioned coordinated control strategy can enable the HESS to achieve adaptive power allocation based on the energy storage margin and obtain an improvement in the hydrogen-to-electricity conversion efficiency of the MFCS.

**Keywords:** DC microgrid; electric–hydrogen coupled; hybrid energy storage system; multistack fuel cell system; power allocation



**Citation:** Li, J.; Liang, C.; Shi, Z. A Coordinated Control Strategy for Efficiency Improvement of Multistack Fuel Cell Systems in Electric–Hydrogen Hybrid Energy Storage System. *Batteries* **2024**, *10*, 331. https://doi.org/10.3390/batteries10090331

Academic Editor: Manickam Minakshi

Received: 24 June 2024
Revised: 3 August 2024
Accepted: 14 August 2024
Published: 19 September 2024



## 1. Introduction

A microgrid is a form of distributed energy supply that effectively integrates renewable energy, energy storage systems, and multiple loads and has greatly promoted the construction of new power systems [1,2]. Renewable energy, such as wind power and photovoltaic power generation, is easily affected by the environment, and its power generation is uncertain and uncontrollable. Therefore, the rational application of energy storage systems and their coordinated control strategy are of great significance for the efficiency and stability of microgrids. A hybrid energy storage system (HESS) composed of hydrogen fuel cells and batteries is a typical energy storage combination used to support the smooth operation of microgrids, which combines the advantages of hydrogen energy storage systems that have a large capacity and long discharge time and the advantages of a battery energy storage system (BESS) with flexible and fast power regulation [3,4]. In actual operation, the power throughput capacity of an HESS is closely related to the level of hydrogen (LoH) in the hydrogen storage tank and the state of charge (SoC) of the battery. In order to give full play to the power response capability of the HESS, it is also necessary to manage the energy of the electric–hydrogen coupled microgrid, coordinate the operation mode of the HESS equipment, and reasonably allocate its operating power. In addition, to solve the problems of low power level, insufficient durability, and limited large-scale application of the current single-stack fuel cell system (FC), an FC is often put into microgrids in the form of multistack array in engineering projects to enhance the

overall operation stability and scalability of the hydrogen energy storage system. However, optimizing the power allocation of the FC so that the multistack fuel cell system (MFCS) can operate at the maximum efficiency point as much as possible is still a key problem that needs to be solved in electric–hydrogen coupled systems.

Multi-energy storage systems can achieve energy interconnection and complementarity and improve energy utilization efficiency and power supply stability. However, the increase in the types of energy storage devices also makes energy management and coordinated control more complicated. In terms of an HESS's energy management, mainstream methods mainly focus on rule-based and optimization control strategies. Refs. [5,6] proposed a minimum hydrogen consumption energy management strategy based on fuzzy logic control (FLC) for HESS. This strategy dynamically adjusts the penalty factor according to the lithium battery SoC, changes the power distribution of the HESS, and, thus, reduces power fluctuations and hydrogen consumption of the fuel cell system. After comparing a large number of optimization algorithms, such as external energy maximization strategy (EEMS), cuckoo search (CS), and grey wolf optimizer (GWO), Ref. [7] selected the Harris Hawks optimizer (HHO) to manage the fuel cell/PV/battery/supercapacitor hybrid energy storage system. The HHO improves the system's operational efficiency while reducing hydrogen consumption by reasonably allocating power among multiple devices.

Overall, rule-based control strategies can simplify the coordinated control of multisystems and have a high degree of adaptability to different operating conditions of microgrids, but their actual application effect depends on engineering experience. The ability of the optimal control strategy to conduct global multi-objective optimization of a system depends on the degree to which the meta-heuristic algorithm explores and utilizes the search space. The selection of an optimization control strategy that is compatible with the system, makes the search range as comprehensive as possible, avoids falling into local optimality, makes full use of the optimal solution that has been searched, distinguishes the effective search range, and accelerates convergence to improve the speed at which a solution is found is difficult to implement [8–10].

In the above research on HESSs, it is not difficult to find that most studies regard fuel cell systems as a whole research object. However, in actual application scenarios with fuel cell systems, such as transportation, aviation, and energy systems [11,12], the power level of the FC often makes it difficult to meet a scenario's requirements, which further promotes scholars' research on MFCSs. Ref. [13] analyzed the advantages and disadvantages of the four electrical architectures of MFCSs, namely, series, parallel, cascade, and series-parallel, in terms of voltage level, fault isolation, control form, and operating efficiency, providing a reference for other scholars in the selection of an appropriate MFCS architecture according to the research scenario. Refs. [14,15] studied the dynamic characteristics of an FC and found that the smaller the change in an FC's output current and the lower the dynamic loading rate, the better the stack's performance, life, and stability. For the device control of an FC, Ref. [16] proposed an adaptive current distribution method to mitigate the performance degradation of the FC and maintain the overall performance consistency of the MFCS.

It can be seen that reasonable energy management strategies should be formulated to avoid the degradation of the overall performance of the MFCS due to excessive use or loss of the FC. Ref. [17] pointed out that after long-term use the output capacity, efficiency, hydrogen consumption, and other performance indicators of fuel cells will decline. Therefore, an energy management strategy with an adaptive adjustment capability for fuel cell attenuation was proposed in this reference, so that the fuel cell has the lowest energy consumption and the best durability performance over its life cycle. Considering the impact of the environment on an MFCS, Ref. [18] proposed a coordinated optimization allocation strategy for an MFCS based on the concept of maximum efficiency range, which not only makes optimal power allocation for FC but also improves the hydrogen-to-electricity conversion efficiency of the MFCS. Ref. [19] proposed an optimal allocation strategy for the power demand of the MFCS, which reduced hydrogen consumption by optimizing the

total output current of the MFCS. After comparing two classic power allocation methods for an MFCS, equidistribution (ED) and daisy chain, Ref. [20] proposed an optimization algorithm that makes the efficiency of the MFCS close to the best efficiency of the FC in a large power range.

It should be noted that although existing power allocation strategies for an MFCS have achieved improvements in efficiency or hydrogen consumption through simple start–stop control or optimized control, most of them assume that the FCs in MFCSs are similar during implementation and have almost no individual differences in performance, power level, etc. Therefore, it is still necessary to explore a control strategy based on the individual differences in FCs to optimize the overall performance of the MFCS. In fact, there is a certain correlation between the output power of the FC and the hydrogen-to-electricity conversion efficiency. Reasonable adjustment of the output power of the FC can allow it to operate at peak efficiency [21,22]. Refs. [23,24] considered the FC differences between stacks and used an optimization algorithm to optimize the power allocation of the FC, thereby achieving the goal of improving the operating efficiency of the MFCS. However, the operational process of an MFCS control strategy based on the optimization algorithm is relatively complicated, and the optimization effect is closely related to the selection of the algorithm; in addition, when microgrid operational objectives or operation modes change, such methods lack rapid adaptability and portability. The perturbation and observation method (P&O) is often used to track the maximum power point in photovoltaic power generation systems [25,26]. This method is simple and easy to implement, and the adjustment of operating constraints and the setting of initial disturbance values are relatively flexible. It can be adapted to various power allocation strategies and has certain portability and superposition of optimization effects. Therefore, it is also widely used in tracking extreme points in the nonlinear characteristic curves of other systems [27,28].

Combined with the above research, this paper took the electric–hydrogen coupled DC microgrid as the research background and proposed a two-layer coordinated control strategy for the HESS. Compared with existing studies, this paper makes improvements in the following aspects:

(1) The upper-layer control strategy takes the overall LoH of the MFCS and the SoC of the battery as indicators and formulates a system-level fuzzy logic control (FLC) rule to complete the initial power allocation between the MFCS and BESS so that different energy storage systems can maintain an appropriate energy storage margin, as much as possible, when smoothing the power shortage of the microgrid.
(2) The lower-layer control strategy considers the LoH of the FC to formulate a device-level FLC rule so as to achieve the initial division of the MFCS overall power into the inter-stack FC power and maintain the consistency of the FC energy storage margin during the discharge process.
(3) A strategy for optimization by perturbation (OP) is proposed based on the power-efficiency characteristics of the FC. The initial power allocation of the FC is adjusted by OP to improve the hydrogen-to-electricity conversion efficiency of the MFCS. In addition, the adaptability of OP to different power allocation strategies is further studied.

This paper aims to realize adaptive power allocation from the system to the device in an HESS and from the array to single stack in an MFCS through a top-down energy management strategy so as to improve the energy autonomy, regulation flexibility, and operation stability of the DC microgrid. Finally, this paper will verify the feasibility and effectiveness of the proposed HESS-coordinated control strategy through simulation and experiments.

## 2. Electric–Hydrogen Coupled DC Microgrid Model

### 2.1. Electric–Hydrogen Coupled DC Microgrid Structure

The structure of the electric–hydrogen coupled DC microgrid studied in this paper is shown in Figure 1, which includes a photovoltaic system, electrolytic hydrogen production system, load, MFCS, and BESS. Each system is connected to the DC bus through a power

electronic converter and is uniformly controlled by the energy management system (EMS). The HESS is composed of the MFCS and BESS. When the power supply of the DC microgrid is tight, energy storage systems cooperate to compensate for the power shortage and maintain the smooth operation of the microgrid. The MFCS is composed of multiple FCs. In order to play its role better in power regulation, the topology of the structure needs to be fully considered. Common MFCS topologies with converters include series, parallel, cascade, and series-parallel structures. The series structure is relatively simple and can reduce the number of converters used in the entire MFCS, but since it has no bypass circuit, a failure of one FC will paralyze the entire MFCS [29]. In the parallel structure [30] and cascade structure [31], the FC and converter are connected to the DC bus in a one-to-one manner, which can realize independent control of the FC. However, considering that the parallel structure has the advantages of a simple structure and low control difficulty compared with the cascade structure, this paper finally selected an MFCS with a three-stack parallel structure as the research object.

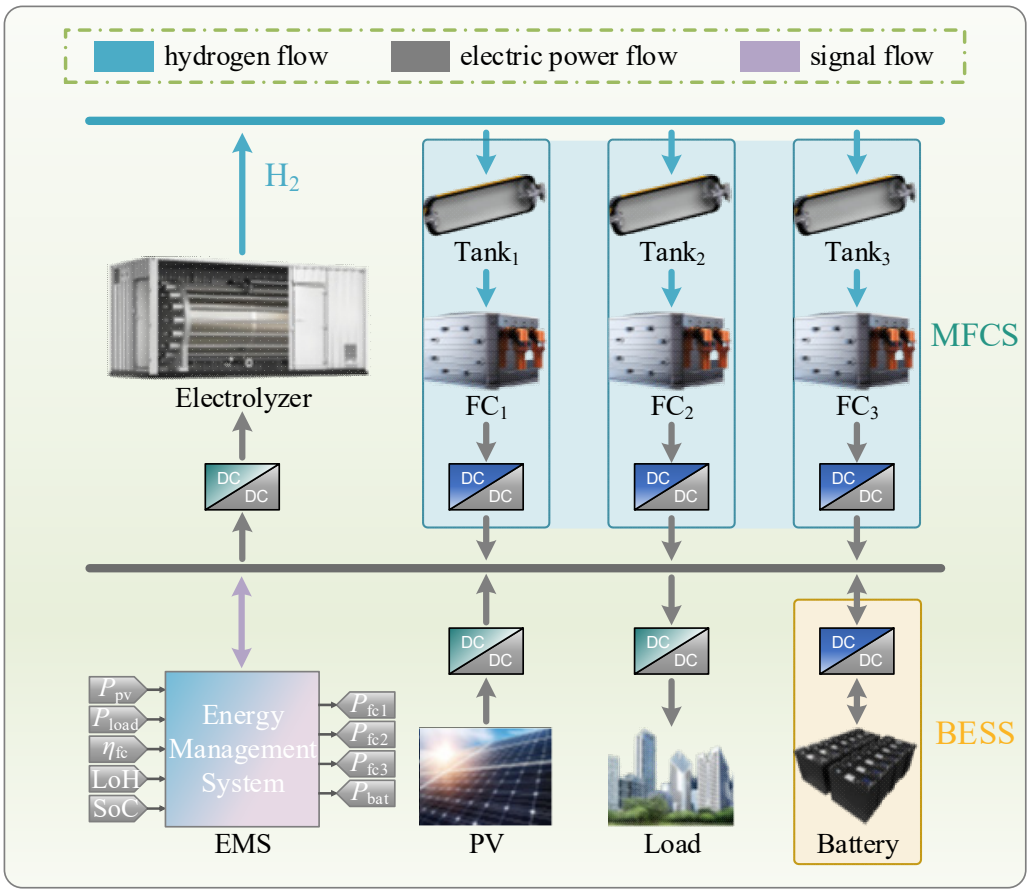


**Figure 1.** Electric–hydrogen coupled DC microgrid structure diagram.

### *2.2. Modeling of the HESS*

#### 2.2.1. Mathematical Model of BESS

The main body of the BESS system is batteries; its model construction method is detailed in the literature [32]. The current conventional measurement methods for the SoC include the coulomb counting method and the voltage method. These methods are based on the measurements of battery voltage and current. There are also methods, such as electrochemical impedance spectroscopy and ultrasonic reflection wave joint estimation, that rely on instrument measurements. These methods can achieve nondestructive measurements of the battery system [33] but are highly sensitive to temperature. Considering that the Coulomb counting method is more convenient, and this article mainly controls

the devices by adjusting the current or voltage, the Coulomb counting method shown in Equation (1) is finally selected to calculate the *SoC*.

$$SoC = SoC_0 - \frac{1}{CU_{\mathrm{bat},t}} \int P_{\mathrm{bat},t} \mathrm{d}t \tag{1}$$

where $SoC_0$ is the initial value of *SoC*; *C* is the rated capacity of battery; $U_{\mathrm{bat},t}$ is the voltage of the battery at time *t*; and $P_{\mathrm{bat},t}$ is the power of the battery at time *t*.

#### 2.2.2. Mathematical Model of Fuel Cell System

A proton exchange membrane fuel cell (PEMFC) has the advantages of a high energy conversion efficiency, fast start–stop speed, and clean and low emissions. Therefore, the FC type selected in this paper was a PEMFC, and its mathematical model is shown in Equation (2) [34,35], as follows:

$$\begin{cases} U_{\mathrm{fc}} = n_{\mathrm{sfc}}(E_{\mathrm{rev\_fc}} - U_{\mathrm{act\_fc}} - U_{\mathrm{ohm\_fc}} - U_{\mathrm{conc\_fc}}) \\ E_{\mathrm{rev\_fc}} = 1.229 - 0.85 \times 10^{-3}(T_{\mathrm{fc}} - 298.15) + 4.3085 \times 10^{-5} T_{\mathrm{fc}} \left[ \ln(p_{\mathrm{H_2}}) + \frac{1}{2} \ln(p_{\mathrm{O_2}}) \right] \\ U_{\mathrm{act\_fc}} = \zeta_1 + \zeta_2 T_{\mathrm{fc}} + \zeta_3 T_{\mathrm{fc}} \ln(I_{\mathrm{fc}}) + \zeta_4 T_{\mathrm{fc}} \ln(C_{\mathrm{O_2}}) \\ C_{\mathrm{O_2}} = \frac{p_{\mathrm{O_2}}}{5.08 \times 10^6 \exp\left(\frac{-498}{T_{\mathrm{fc}}}\right)} \\ U_{\mathrm{ohm\_fc}} = I_{\mathrm{fc}} \left( \frac{\rho_{\mathrm{M}} l}{A} + R_{\mathrm{c}} \right) \\ U_{\mathrm{conc\_fc}} = -B \ln\left(1 - \frac{J}{J_{\max}}\right) \end{cases} \tag{2}$$

where $U_{\mathrm{fc}}$ is the voltage of the FC; $n_{\mathrm{sfc}}$ is the number of fuel cell chips connected in series; $E_{\mathrm{rev\_fc}}$ is the reversible voltage; $U_{\mathrm{act\_fc}}$ is the activation overvoltage; $U_{\mathrm{ohm\_fc}}$ is the ohmic overvoltage; $U_{\mathrm{conc\_fc}}$ is the concentration difference overvoltage; $T_{\mathrm{fc}}$ is the Kelvin temperature of the FC; $p_{\mathrm{H_2}}$ is the anode hydrogen partial pressure; $p_{\mathrm{O_2}}$ is the cathode oxygen partial pressure; $\zeta_1$, $\zeta_2$, $\zeta_3$, and $\zeta_4$ are the empirical parameters; $I_{\mathrm{fc}}$ is the current of the FC; $C_{\mathrm{O_2}}$ is the oxygen solubility at the gas–liquid interface; $\rho_{\mathrm{M}}$ is the resistivity of the proton exchange membrane; *l* is the thickness of the proton exchange membrane; *A* is the effective activation area of the proton exchange membrane; $R_{\mathrm{c}}$ is the resistance that prevents protons from passing through the proton exchange membrane; *B* is a constant; *J* is the current density of the FC; and $J_{\max}$ is the maximum current density of the FC.

The calculation formula of the LoH of the *i*-th FC ($\mathrm{FC}_i$) is shown in Equation (3) ($i$ = 1, 2, 3).

$$LoH_{\mathrm{fc}i} = \frac{p_{\mathrm{tank}i}}{p_{\mathrm{tank\_max}i}} \times 100\% \tag{3}$$

where $LoH_{\mathrm{fc}i}$ is the LoH of the $\mathrm{FC}_i$; $p_{\mathrm{tank}i}$ is the internal pressure of the hydrogen storage tank connected to the $\mathrm{FC}_i$; $p_{\mathrm{tank\_max}i}$ is the maximum internal pressure that the hydrogen storage tank connected to the $\mathrm{FC}_i$ can withstand.

The LoH of the MFCS is determined by the LoH of all FCs. Since the capacity, working pressure, and other parameters of the hydrogen storage tanks used in this paper are consistent, the LoH calculation formula of the MFCS can be inferred, as shown in Equation (4).

$$LoH_{\mathrm{mfcs}} = \frac{LoH_{\mathrm{fc1}} + LoH_{\mathrm{fc2}} + LoH_{\mathrm{fc3}}}{3} \tag{4}$$

where $LoH_{\mathrm{mfcs}}$ is the LoH of the MFCS.

#### 2.2.3. Model of Hydrogen-to-Electricity Conversion Efficiency for Fuel Cell Systems

The hydrogen-to-electricity conversion of the FC is completed by the fuel cell stack, auxiliary equipment, and other equipment, involving intermediate processes such as thermoelectric conversion, power conversion, and fuel utilization [36]. The calculation formula for the hydrogen-to-electricity conversion efficiency of the $\mathrm{FC}_i$ is shown in Equation (5).

$$\begin{cases} \eta_{\mathrm{fc}i} = \eta_{\mathrm{stack}i}\eta_{ei}\eta_{\mathrm{fuel}i} \\ \eta_{\mathrm{stack}i} = \frac{U_{\mathrm{sfc}i}}{\Delta H/(2F)} \times 100\% \\ \eta_{ei} = \frac{P_{\mathrm{out}i} - P_{\mathrm{aux}i}}{P_{\mathrm{out}i}} \times 100\% \end{cases} \quad (5)$$

where $\eta_{\mathrm{fc}i}$ is the hydrogen-to-electricity conversion efficiency of the $\mathrm{FC}_i$; $\eta_{\mathrm{stack}i}$ is the thermoelectric conversion efficiency of the $\mathrm{FC}_i$ stack; $\eta_{ei}$ is the power conversion efficiency of the $\mathrm{FC}_i$; $\eta_{\mathrm{fuel}i}$ is the hydrogen fuel utilization rate of the $\mathrm{FC}_i$; $U_{\mathrm{sfc}i}$ is the output voltage of the $\mathrm{FC}_i$ stack; $\Delta H$ is the calorific value of hydrogen; $F$ is the Faraday constant; $P_{\mathrm{out}i}$ is the output power of the $\mathrm{FC}_i$ stack; and $P_{\mathrm{aux}i}$ is the electric power consumed by the $\mathrm{FC}_i$ auxiliary machine.

Combined with Equation (5), Figure 2 depicts the hydrogen-to-electricity conversion efficiency curves of the FCs of three power levels.

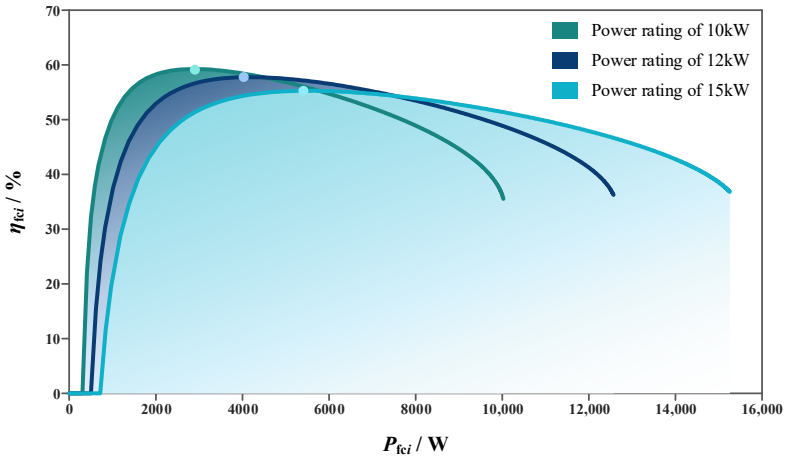


**Figure 2.** Hydrogen–electric conversion efficiency curves of the FC.

It can be seen from Figure 2 that the hydrogen-to-electricity conversion efficiency of the FC increased rapidly at first and then decreased slowly with the increase in the stack output power, with an efficiency peak. It can also be observed that because of individual differences in FCs, their hydrogen-to-electricity conversion efficiency curves are also different. In practical applications, factors such as power level, battery performance, and working conditions will affect the hydrogen-to-electricity conversion efficiency of the FC. It is difficult to optimize the efficiency of all FCs and MFCS simultaneously through a unified FC power allocation value. Therefore, in order to further study the output power distribution of the $\mathrm{FC}_i$ when MFCS operates at maximum efficiency, it is also necessary to define the hydrogen-to-electricity conversion efficiency of the MFCS as shown in Equation (6).

$$\eta_{\mathrm{mfcs}} = \frac{P_{\mathrm{fc1}} + P_{\mathrm{fc2}} + P_{\mathrm{fc3}}}{\frac{P_{\mathrm{fc1}}}{\eta_{\mathrm{fc1}}} + \frac{P_{\mathrm{fc2}}}{\eta_{\mathrm{fc2}}} + \frac{P_{\mathrm{fc3}}}{\eta_{\mathrm{fc3}}}} \quad (6)$$

where $\eta_{\mathrm{mfcs}}$ is the hydrogen-to-electricity conversion efficiency of the MFCS; $P_{\mathrm{fc}i}$ is the output power of the $\mathrm{FC}_i$; and $\eta_{\mathrm{fc}i}$ is the hydrogen-to-electricity conversion efficiency of the $\mathrm{FC}_i$.

## 3. Coordinated Control Strategy for Electric–Hydrogen Hybrid Energy Storage System

The voltage and power balance equations of the electric–hydrogen coupled DC microgrid are shown in Equation (7).

$$\begin{cases} C_{\mathrm{dc}}\frac{\mathrm{d}U_{\mathrm{dc}}}{\mathrm{d}t} = I_{\mathrm{pv}} + I_{\mathrm{mfcs}} \pm I_{\mathrm{bat}} - I_{\mathrm{load}} \\ \frac{1}{2}C_{\mathrm{dc}}\frac{\mathrm{d}U_{\mathrm{dc}}^2}{\mathrm{d}t} = P_{\mathrm{pv}} + P_{\mathrm{mfcs}} \pm P_{\mathrm{bat}} - P_{\mathrm{load}} \end{cases} \quad (7)$$

where $C_{dc}$ is the bus capacitor; $U_{dc}$ is the bus voltage; $I_{pv}$ is the PV system current; $I_{mfcs}$ is the MFCS current; $I_{bat}$ is the BESS current; $I_{load}$ is the load current; $P_{pv}$ is the PV system power; $P_{mfcs}$ is the MFCS power; $P_{bat}$ is the BESS power; and $P_{load}$ is the load power.

Equation (7) shows that the premise of microgrid bus voltage stability is the balance between the load and the total power of each micro-source, as shown in Equation (8). The key to microgrid energy management is to smooth the unbalanced power, $P_{net}$, of the microgrid through the HESS, that is, to reasonably allocate the power of the MFCS and BESS, as well as the power of the $FC_i$.

$$\begin{cases} P_{net} = P_{load} - P_{pv} = P_{mfcs} \pm P_{bat} \\ P_{mfcs} = P_{fc1} + P_{fc2} + P_{fc3} \end{cases} \tag{8}$$

In order to maintain the stable operation of the microgrid through the coordinated control of the HESS, this paper proposes a two-layer control strategy for the HESS, as shown in Figure 3. The upper-layer control comprehensively considers the charge and discharge margin of the HESS and uses FLC to realize the initial power allocation of the MFCS and BESS. The lower-layer control combines the FC operational characteristics, takes the MFCS's hydrogen-to-electricity conversion efficiency as the goal, further divides the power of the $FC_i$, and appropriately adjusts the final allocated power of the MFCS and BESS so that the overall output value of the HESS remains unchanged before and after the adjustment.

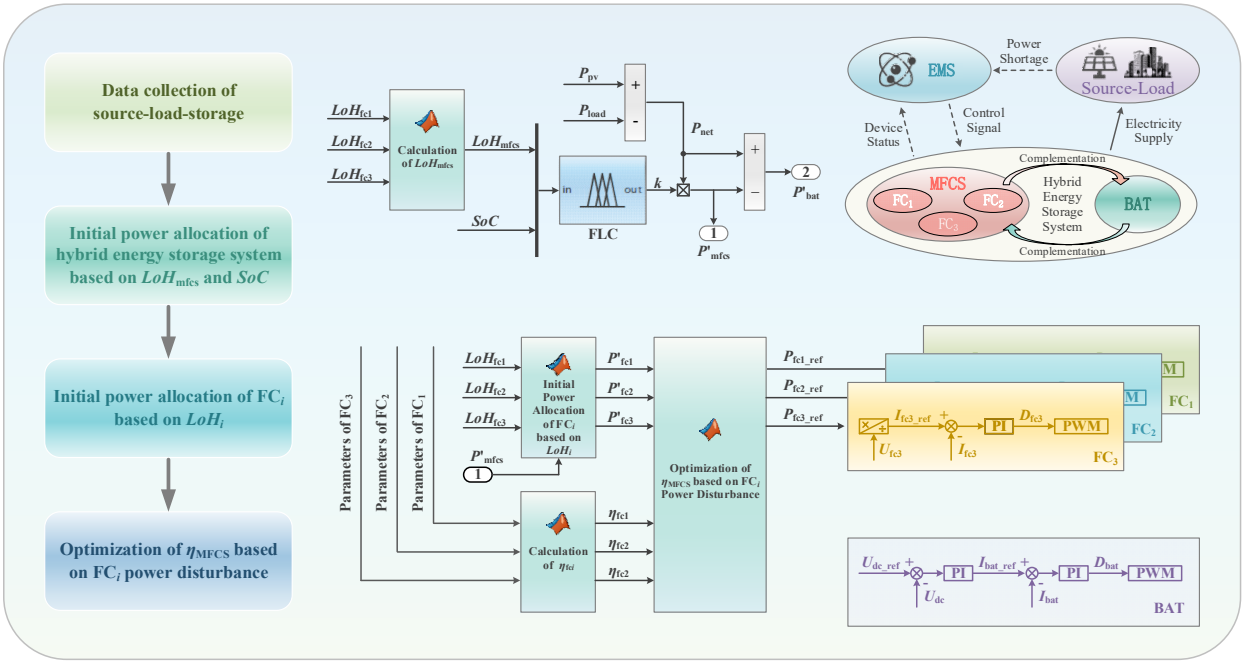


**Figure 3.** The two-layer control principle of the HESS.

In addition, in order to make the control of the MFCS and BESS devices more accurate and stable, this paper adopted current loop control for the FC and voltage-current dual closed-loop control for the battery in the BESS [37]. In Figure 3, $P_{fci\_ref}$ is the output power reference value of the $FC_i$; $U_{fci}$ is the output voltage of the $FC_i$; $I_{fci}$ is the output current of the $FC_i$; $I_{fci\_ref}$ is the output current reference value of the $FC_i$; $D_{fci}$ is the duty cycle signal acting on the DC/DC converter connected to the $FC_i$; $P_{bat\_ref}$ is the output power reference value of the battery; $U_{dc\_ref}$ is the bus voltage reference value, $I_{bat}$ is the output current of the battery, $I_{bat\_ref}$ is the output current reference value of the battery; and $D_{bat}$ is the duty cycle signal acting on the DC/DC converter connected to the battery.

### *3.1. Adaptive Power Allocation of the HESS Based on FLC*

FLC is a control method based on customized rules. It has the advantages of strong robustness, high reliability, and fast response in the face of complex control systems [38]. Considering the time-varying and irregular combinations of parameters, such as $P_{net}$, $LoH_{mfcs}$, and $SoC$, during the microgrid's operation, the use of FLC can quickly adapt to the multiple operating conditions of the microgrid and make precise adjustments to the control parameters.

The power adaptive allocation principle of the HESS is to allocate $P_{net}$ to MFCS and BESS based on their actual charging and discharging margins during operation. Specifically, an initial power allocation factor, $k$, is introduced. The value of $k$ is adjusted in real time according to the state of the $LoH_{mfcs}$ and $SoC$ in the current microgrid's operation so that the energy storage system with a large energy storage margin is given priority to output. The $LoH_{mfcs}$ and $SoC$ are maintained in a reasonable output range before and after output so as to avoid excessive output of a single energy storage system affecting its safety or life [39].

According to the above rule-making principles, this paper formulates a fuzzy logic rule table with $LoH_{mfcs}$ and $SoC$ as dual input variables and the MFCS power allocation factor $k$ as a single output variable, as shown in Table 1, and sets the membership function, as shown in Figure 4.

**Table 1.** Fuzzy logic rules for power allocation of the HESS.

| ***K*** | | ***SoC*** | | | | |
|---|---|---|---|---|---|---|
| | | **VS** | **S** | **M** | **B** | **VB** |
| $\boldsymbol{LoH_{mfcs}}$ | VS | M | S | S | VS | VS |
| | S | B | M | S | S | S |
| | M | B | B | M | S | VS |
| | B | VB | B | M | M | M |
| | VB | VB | VB | B | M | M |

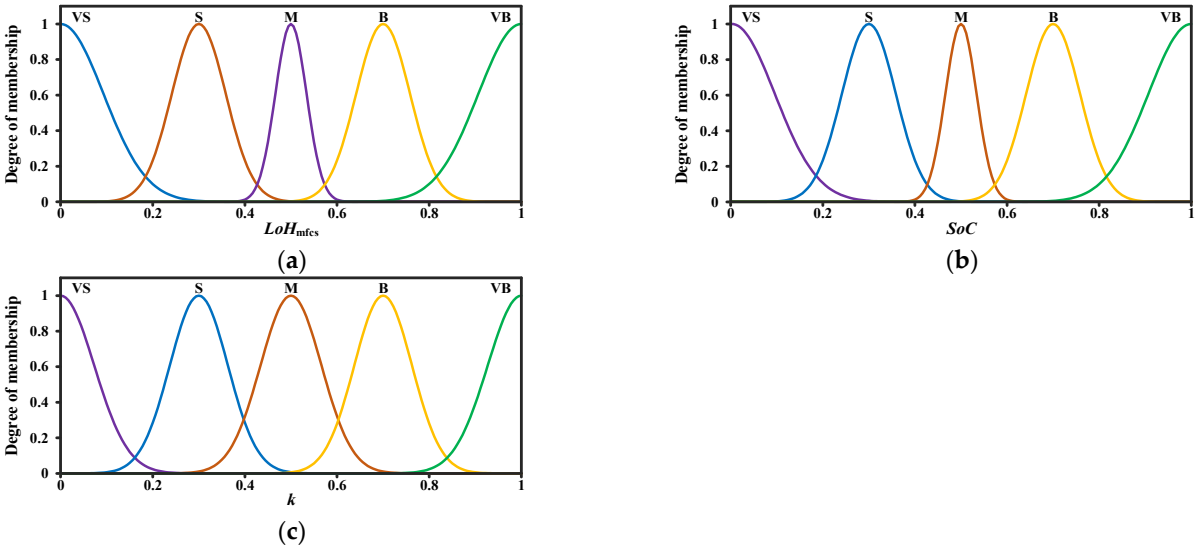


**Figure 4.** Membership functions for the power allocation of the HESS: (**a**) Membership function of $LoH_{mfcs}$; (**b**) Membership function of $SoC$; (**c**) Membership function of $k$.

According to the initial power allocation factor, $k$, solved by FLC, the initial power allocation of the MFCS and BESS can be further obtained, as shown in Equation (9).

$$\begin{cases} P'_{mfcs} = k \cdot P_{net} \\ P'_{bat} = P_{net} - P'_{mfcs} \end{cases} \quad (9)$$

where $P'_{\mathrm{mfcs}}$ is the initial power allocation of the MFCS, and $P'_{\mathrm{bat}}$ is the initial power allocation of BESS.

### *3.2. Optimization of the MFCS Efficiency Based on FC Power Perturbation*

Using $LoH_{\mathrm{mfcs}}$ and *SoC* as the basis for power allocation can keep MFCS and BESS in a reasonable operating range, as much as possible, during operation and retain a certain energy storage margin. However, in actual operation, the energy storage system needs to be fully utilized to ensure the economy and efficiency of the microgrid. The hydrogen-to-electricity conversion efficiency of the FC is closely related to its operating power. Therefore, the problem of how to improve the efficiency of the MFCS by adjusting the power distribution of the $\mathrm{FC}_i$ has its research value. To achieve the above objectives, this paper proposes an MFCS efficiency optimization strategy based on FC power perturbation (OP for short), and the implementation steps are shown in Figure 5. The core steps of this strategy can be divided into the following two parts: calculation of the MFCS's initial efficiency and optimization of the MFCS efficiency based on FC power perturbation.

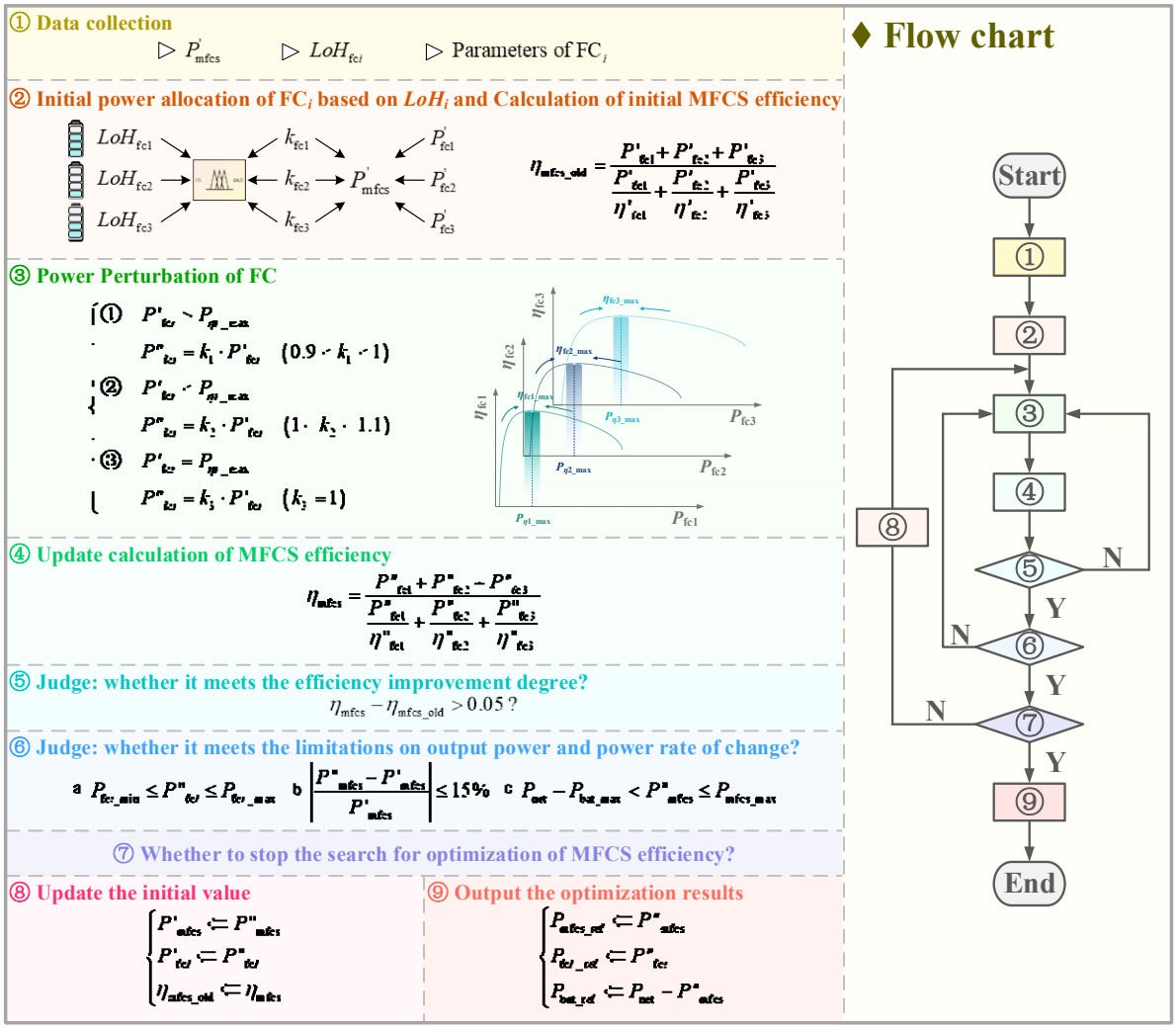


**Figure 5.** Flow chart of OP.

#### 3.2.1. Calculation of Initial Value of the MFCS Efficiency

The prerequisite for calculating the MFCS's efficiency is clarifying the output power and corresponding efficiency of the $\mathrm{FC}_i$. Similar to the power allocation principle of the MFCS and BESS, the power allocation of the $\mathrm{FC}_i$ is based on its energy storage margin. FLC will be used to allocate the power from MFCS to $\mathrm{FC}_i$. Specifically, the single-stack power

allocation factor $k'_I$ is introduced, and the value of $k'_I$ is adjusted according to the state of the $LoH_i$ so that the $FC_i$ with a large $LoH_i$ is given priority to output more power.

The initial power allocation of the $FC_i$ is shown in Equation (10). The corresponding three-input and three-output fuzzy logic rules table is shown in Table 2, and the membership functions are shown in Figure 6.

$$P'_{fci} = k'_i \cdot P'_{mfcs} \tag{10}$$

**Table 2.** Fuzzy logic rules for power allocation of the $PEMFC_i$.

| $LoH_{fc1}$, $LoH_{fc2}$, $LoH_{fc3}$ | $k_{fc1}$, $k_{fc2}$, $k_{fc3}$ | $LoH_{fc1}$, $LoH_{fc2}$, $LoH_{fc3}$ | $k_{fc1}$, $k_{fc2}$, $k_{fc3}$ | $LoH_{fc1}$, $LoH_{fc2}$, $LoH_{fc3}$ | $k_{fc1}$, $k_{fc2}$, $k_{fc3}$ |
|---|---|---|---|---|---|
| S, S, S | M, M, M | M, S, S | B, S, S | B, S, S | B, S, S |
| S, S, M | S, S, B | M, S, M | M, S, M | B, S, M | B, S, M |
| S, S, B | S, S, B | M, S, B | M, S, B | B, S, B | B, S, B |
| S, M, S | S, B, S | M, M, S | M, M, S | B, M, S | B, M, S |
| S, M, M | S, B, B | M, M, M | M, M, M | B, M, M | B, M, M |
| S, M, B | S, M, B | M, M, B | M, M, B | B, M, B | B, M, B |
| S, B, S | S, B, S | M, B, S | M, B, S | B, B, S | B, B, S |
| S, B, M | S, B, M | M, B, M | M, B, M | B, B, M | B, B. M |
| S, B, B | S, B, B | M, B, B | M, B, B | B, B, B | B, B, B |

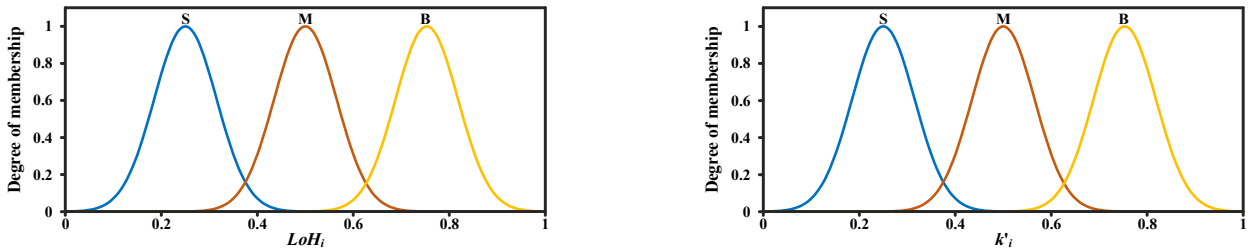


(**a**) (**b**)

**Figure 6.** Membership functions for power allocation of the FC: (**a**) Membership function of $LoH_i$; (**b**) Membership function of $k'_i$.

In order to avoid the collaborative control delay to the HESS caused by the slow real-time calculation speed of $\eta_{fci}$, this paper adopted the offline calculation method to collect the relevant operating parameters of the $FC_i$ in advance, calculate the hydrogen-to-electricity conversion efficiency corresponding to different output powers of the $FC_i$, and store the results. Therefore, when the initial value of the MFCS efficiency, $\eta_{mfcs\_old}$, under the initial power allocation of the $FC_i$ is calculated by Equation (11), $\eta'f_{ci}$ can be found by only mapping $P'_{fci}$ in the offline database.

$$\eta_{mfcs\_old} = \frac{P'_{fc1} + P'_{fc2} + P'_{fc3}}{\frac{P'_{fc1}}{\eta'_{fc1}} + \frac{P'_{fc2}}{\eta'_{fc2}} + \frac{P'_{fc3}}{\eta'_{fc3}}} \tag{11}$$

### 3.2.2. Optimization Process of OP

It can be seen from Equations (6) and (11) that when the efficiency of the $FC_i$ reaches the optimal value, $\eta_{fci\_max}$, the efficiency of the MFCS is also optimized. Therefore, to improve the efficiency of the MFCS, $FC_i$ takes the power value $P_{\eta i\_max}$ corresponding to $\eta_{fci\_max}$ as the power reference point ($\eta_{fci\_max}$ and $P_{\eta i\_max}$ can be obtained from the offline database) and the approximates $P_{\eta i\_max}$ in a perturbation manner based on the current power allocation value $P'_{fci}$. The perturbation rule of the $FC_i$ is shown in Equation (12).

$$\begin{cases} ① & P'_{\mathrm{fc}i} > P_{\eta i\_\max} \\ & P''_{\mathrm{fc}i} = \lambda_1 \cdot P'_{\mathrm{fc}i} \quad (0.9 < \lambda_1 < 1) \\ ② & P'_{\mathrm{fc}i} < P_{\eta i\_\max} \\ & P''_{\mathrm{fc}i} = \lambda_2 \cdot P'_{\mathrm{fc}i} \quad (1 < \lambda_2 < 1.1) \\ ③ & P'_{\mathrm{fc}i} = P_{\eta i\_\max} \\ & P''_{\mathrm{fc}i} = \lambda_3 \cdot P'_{\mathrm{fc}i} \quad (\lambda_3 = 1) \end{cases} \tag{12}$$

where $\lambda_1$, $\lambda_2$, and $\lambda_3$ are the perturbation factors in three different situations, and $P''_{\mathrm{fc}i}$ is the output update value of the $\mathrm{FC}_i$ after perturbation. The efficiency curve of the FC has the characteristic of increasing first and then decreasing. Therefore, when $P'_{\mathrm{fc}i}$ is on the right side of $P_{\eta i\_\max}$, $P'_{\mathrm{fc}i}$ needs to be reduced to make $\eta' \mathrm{f}_{\mathrm{c}i}$ approach $\eta_{\mathrm{fc}i\_\max}$, and $\lambda_1$ takes a random value in the interval (0.9, 1). Similarly, when $P'_{\mathrm{fc}i}$ is on the left side of $P_{\eta i\_\max}$, $\lambda_2$ takes a random value in the interval (1, 1.1); when $P'_{\mathrm{fc}i}$ is exactly equal to $P_{\eta i\_\max}$, $\lambda_3$ takes a value of 1, and no perturbation is required.

Furthermore, the output update value $P''_{\mathrm{mfcs}}$ of the MFCS after the perturbation can be calculated as shown in Equation (13).

$$P''_{\mathrm{mfcs}} = P''_{\mathrm{fc1}} + P''_{\mathrm{fc2}} + P''_{\mathrm{fc3}} \tag{13}$$

The efficiency update value, $\eta_{\mathrm{mfcs}}$, of the MFCS after perturbation is shown in Equation (14).

$$\eta_{\mathrm{mfcs}} = \frac{P''_{\mathrm{fc1}} + P''_{\mathrm{fc2}} + P''_{\mathrm{fc3}}}{\frac{P''_{\mathrm{fc1}}}{\eta''_{\mathrm{fc1}}} + \frac{P''_{\mathrm{fc2}}}{\eta''_{\mathrm{fc2}}} + \frac{P''_{\mathrm{fc3}}}{\eta''_{\mathrm{fc3}}}} \tag{14}$$

To avoid frequent fluctuations in the output power of the MFCS during OP, it is necessary to screen the advantages and disadvantages of the $\eta_{\mathrm{mfcs}}$ and $P''_{\mathrm{fc}i}$. The screening conditions are divided into two levels. The first level is the screening for the efficiency improvement in the MFCS, which requires an improvement in $\eta_{\mathrm{mfcs}}$ by more than 5%. The second level is the restriction on the output value of the $\mathrm{FC}_i$ and MFCS, as shown in Equation (15). The output value of the $\mathrm{FC}_i$ after the perturbation should not exceed its upper and lower limits and should consider the output capacity of the BESS so that after the complementary output of the MFCS and BESS, the requirements of $P_{\mathrm{net}}$ can still be met. Additionally, in order to smoothly adjust the MFCS output and avoid damage to the device caused by large fluctuations in the output value of the energy storage system, it is required that the change rate of the MFCS output value before and after the perturbation should not exceed 15%.

$$\begin{cases} P_{\mathrm{fc}i\_\min} \le P''_{\mathrm{fc}i} \le P_{\mathrm{fc}i\_\max} \\ \left| \frac{P''_{\mathrm{mfcs}} - P'_{\mathrm{mfcs}}}{P'_{\mathrm{mfcs}}} \right| \le 15\% \\ P_{\mathrm{net}} - P_{\mathrm{bat\_max}} < P''_{\mathrm{mfcs}} \le P_{\mathrm{mfcs\_max}} \end{cases} \tag{15}$$

where $P_{\mathrm{fc}i\_\min}$ and $P_{\mathrm{fc}i\_\max}$ are the minimum and maximum outputs of the $\mathrm{FC}_i$, respectively; $P_{\mathrm{bat\_max}}$ is the maximum output of the battery in the BESS; and $P_{\mathrm{mfcs\_max}}$ is the maximum output of the MFCS.

The $P''_{\mathrm{fc}i}$ that satisfies the above two levels of screening can be used as the reference value of the new round of the $\mathrm{FC}_i$ power perturbation and participate in the further optimization of the MFCS's efficiency until the optimization stop instruction is met (such as the sampling interval of EMS is reached). The currently found $P''_{\mathrm{fc}i}$ and $P''_{\mathrm{mfcs}}$ that make the $\eta_{\mathrm{mfcs}}$ optimal are output as the reference values of the $\mathrm{FC}_i$ and MFCS, respectively.

## 4. Simulation Verification

In order to verify the application effect of the strategy proposed in this paper, a model of the HESS with the parameters shown in Table 3 was built with the MATLAB R2022a/Simulink platform.

**Table 3.** Parameter settings for the simulation.

| Device | Variables | Value |
|---|---|---|
| $FC_1$ | $n_{sfc1}$<br>$P_{fc1\_e}$<br>$U_{fc1}$ | 300<br>10 kW<br>425 V |
| $FC_2$ | $n_{sfc2}$<br>$P_{fc2\_e}$<br>$U_{fc2}$ | 420<br>12 kW<br>515 V |
| $FC_3$ | $n_{sfc3}$<br>$P_{fc3\_e}$<br>$U_{fc3}$ | 500<br>15 kW<br>595 V |
| Tank | $p_{tank\_max}$<br>$V_{tank}$ | 25 MPa<br>30 L |
| Battery | $C$<br>$U_{bat\_e}$<br>$P_{bat\_e}$ | 30 Ah<br>300 V<br>30 kW |
| DC Bus | $C_{dc}$<br>$U_{dc}$ | 2000 μF<br>480 V |

### *4.1. Verification of the Power Adaptive Allocation*

The initial power allocation of the $P_{net}$ needs to take into account the $LoH_i$, $LoH_{mfcs}$, and $SoC$ so that the output capacity of each energy storage device is compatible with its energy storage margin. Therefore, in order to verify the effectiveness and feasibility of the FLC-based power adaptive allocation strategy, this section sets up two scenarios for the microgrid's operating environment, as shown in Table 4. In Scenario 1, the initial values of the energy storage margin are different; in scenario 2, the initial values of the energy storage margin are basically the same.

**Table 4.** The runtime environment of the DC microgrid.

| Time (s) | $P_{pv}$ (kW) | $P_{load}$ (kW) |
|---|---|---|
| 0–1 | 3.1 | 10 |
| 1–2 | 4.6 | 15 |
| 2–3 | 6.2 | 25 |
| 3–4 | 3.1 | 25 |
| 4–5 | 7.8 | 25 |

#### 4.1.1. Scenario 1

The initial values of the energy storage margin of the devices in Scenario 1 are different, so this paper set the values of the $LoH_i$, $LoH_{mfcs}$, and $SoC$ as shown in Table 5. The corresponding simulation results of the power of photovoltaic, load, HESS, and the simulation result of bus voltage are shown in Figure 7a; the $LoH_i$ simulation results of the $FC_i$ are shown in Figure 7b.

**Table 5.** Initial parameters of the devices in Scenario 1.

| $LoH_{fc1}$ | $LoH_{fc2}$ | $LoH_{fc3}$ | $LoH_{mfcs}$ | $SoC$ |
|---|---|---|---|---|
| 0.75 | 0.5 | 0.25 | 0.5 | 0.7 |

As can be seen from Figure 7, the $P_{net}$ compensation amount undertaken by the BESS is higher than that of the MFCS. For the single-stack power allocation of the MFCS, the $FC_i$ output value was positively correlated with the $LoH_i$. At the same time, in the same period, the $LoH_i$ drop in the $FC_i$ with a higher $LoH_i$ was greater, and the $LoH_i$ drop in the $FC_i$ with

a lower $LoH_i$ was lower, which also reflects that the discharge rate of the $FC_i$ is related to the range of $LoH_i$.

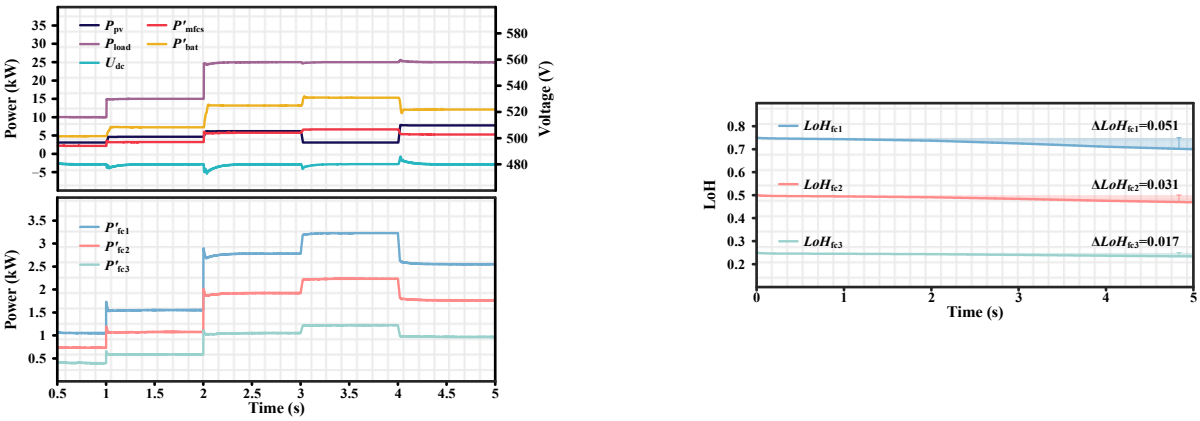


(**a**) (**b**)

**Figure 7.** Simulation results of Scenario 1: (**a**) Power of devices and bus voltage; (**b**) LoH of the $FC_i$.

It can also be found that although the PV and load conditions are constantly changing in the microgrid's operating environment, the microgrid, as a whole, satisfies the supply–demand balance by coordinating the output of the HESS through the FLC strategy so that the DC bus voltage fluctuation is less than 1.5%.

#### 4.1.2. Scenario 2

The initial values of the energy storage margin of the devices in Scenario 2 are basically the same. This paper set the values of the $LoH_i$, $LoH_{mfcs}$, and $SoC$ as shown in Table 6. The corresponding simulation results of the power of the photovoltaic, load, HESS, and the simulation result of the bus voltage are shown in Figure 8a; the $LoH_i$ simulation results of the $FC_i$ are shown in Figure 8b.

**Table 6.** Initial parameters of the devices in Scenario 2.

| $LoH_{fc1}$ | $LoH_{fc2}$ | $LoH_{fc3}$ | $LoH_{mfcs}$ | $SoC$ |
|---|---|---|---|---|
| 0.45 | 0.5 | 0.55 | 0.5 | 0.3 |

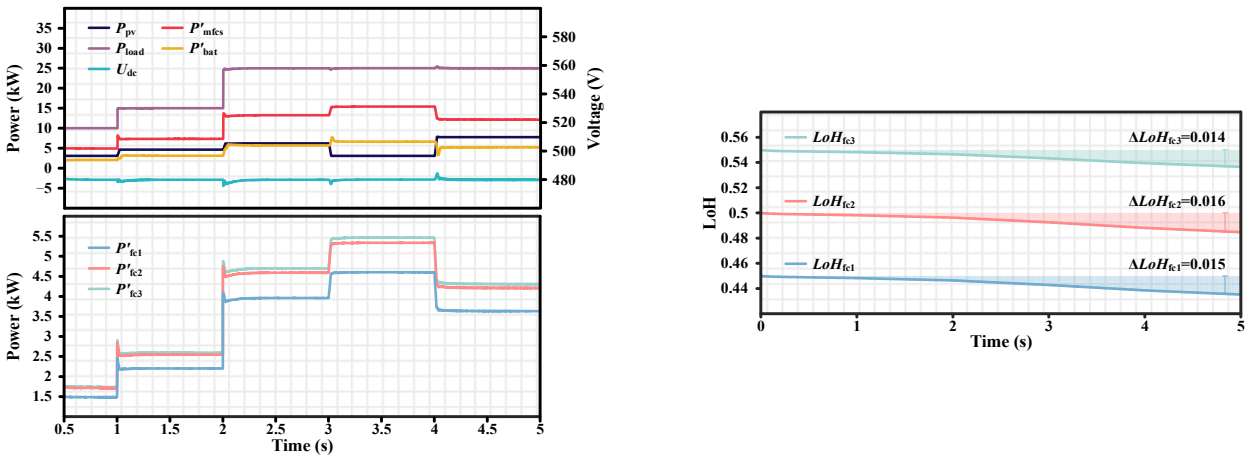


(**a**) (**b**)

**Figure 8.** Simulation results of Scenario 2: (**a**) Power of devices and bus voltage; (**b**) LoH of the $FC_i$.

It can be seen from Figure 8 that the MFCS bears most of the $P_{net}$ compensation. For the single-stack power allocation of the MFCS, the $LoH_i$ of the $FC_i$ is in a reasonable range, so its output value varies slightly with the $LoH_i$, but the discharge rate can be approximately regarded as the same. In addition, the DC bus in Scenario 2 also remained stable, with only a slight fluctuation of less than 0.93% occurring when the microgrid's operating conditions changed.

In summary, the FLC-based primary power allocation strategy enables the HESS to adaptively allocate power according to the energy storage margin of each device in a fluctuating microgrid environment, thereby maintaining the supply and demand balance of the microgrid.

### *4.2. Verification of OP*

Figure 9 shows the operating efficiency of the MFCS with the different combined outputs of the three FC stacks (for ease of observation, $P_{fc3}$ = 8 kW, and only $P_{fc1}$ and $P_{fc2}$ are changed). As shown in Figure 9, when the $P_{fci}$ of each fuel cell stack approaches $P_{\eta i\_max}$, $\eta_{mfcs}$ can also achieve a larger value at the same time. Therefore, on the basis of realizing the initial power allocation, the energy storage system should further consider how to make full use of the MFCS by fine-tuning the power allocation of the $FC_i$. This section will verify the application effect of the OP in improving the efficiency of the MFCS.

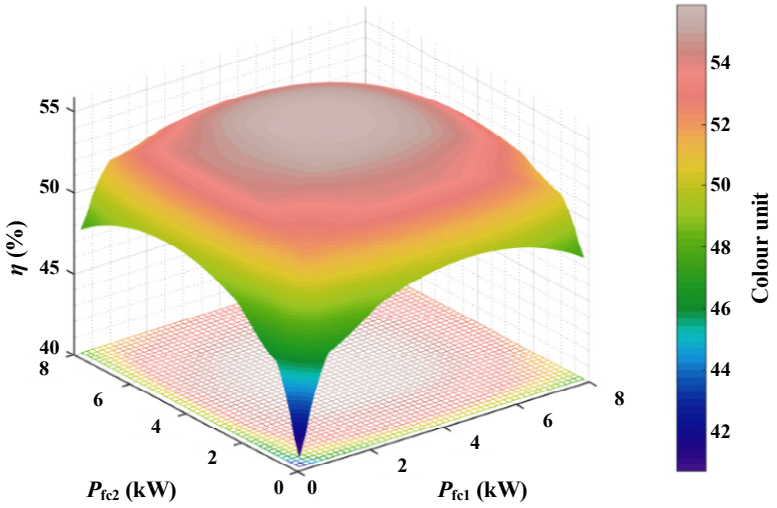


**Figure 9.** Efficiency curve characteristics of the MFCS.

#### 4.2.1. Efficiency Optimization Based on FLC Power Allocation Strategy

Figure 10 compares the operation of the MFCS and $FC_i$ before and after the FLC's initial power allocation strategy superimposed with OP.

In Figure 10a, $\eta_{hist}$ is the MFCS efficiency value corresponding to each perturbation result during the OP process. $\eta_{mfcs}$ and $\eta''_{fci}$ are the efficiency values of the MFCS and $FC_i$ after using OP, respectively. $\eta_{mfcs\text{-}old}$ and $\eta'f_{ci}$ are the corresponding efficiency values when the MFCS and $FC_i$ did not use OP for the initial power allocation given by FLC, respectively. Figure 10b shows the difference in output power before and after the MFCS used OP.

From the operational results of 0–5 s, it can be seen that $\eta_{mfcs}$ was always the optimal value of $\eta_{hist}$ under various operating conditions. Compared with $\eta_{mfcs\text{-}old}$, it can be seen that OP makes the MFCS achieve an efficiency improvement rate of 3.4–9.5%. Synchronously, the efficiency of the $FC_i$ also improved to varying degrees, and the $FC_i$ efficiency improvement rate can reach up to 8.6%. In addition, since OP limits the power fluctuation rate and amplitude of the MFCS, and the output difference of the MFCS can be compensated by the BESS, the power of the MFCS will not fluctuate significantly after using OP, and the bus voltage fluctuation rate did not exceed 0.57%.

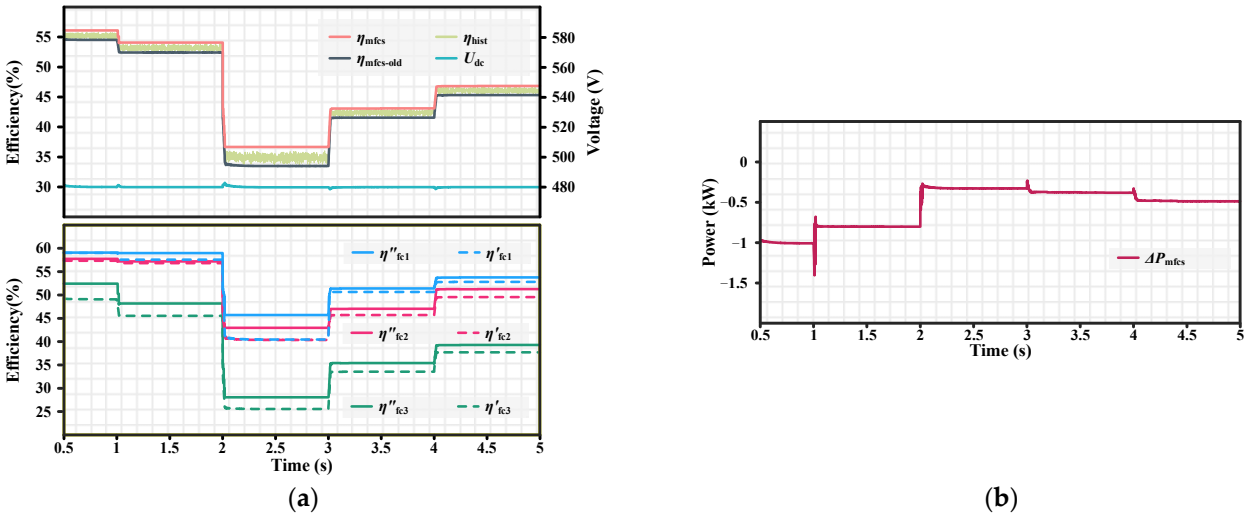


(**a**) (**b**)

**Figure 10.** Results of the OP based on the FLC power allocation strategy: (**a**) Efficiency of MFCS and $FC_i$ and bus voltage; (**b**) Power fluctuation of MFCS.

#### 4.2.2. Efficiency Optimization Based on ED Power Allocation Strategy

In order to explore whether the efficiency improvement effect presented by OP when acting on the FLC strategy is accidental, this section applied OP to the following classic power allocation strategy used by the MFCS: ED (as shown in Equation (16)). The corresponding simulation results are shown in Figure 11.

$$P'_{\mathrm{Fc}i} = \frac{P'_{\mathrm{mfcs}}}{3} \tag{16}$$

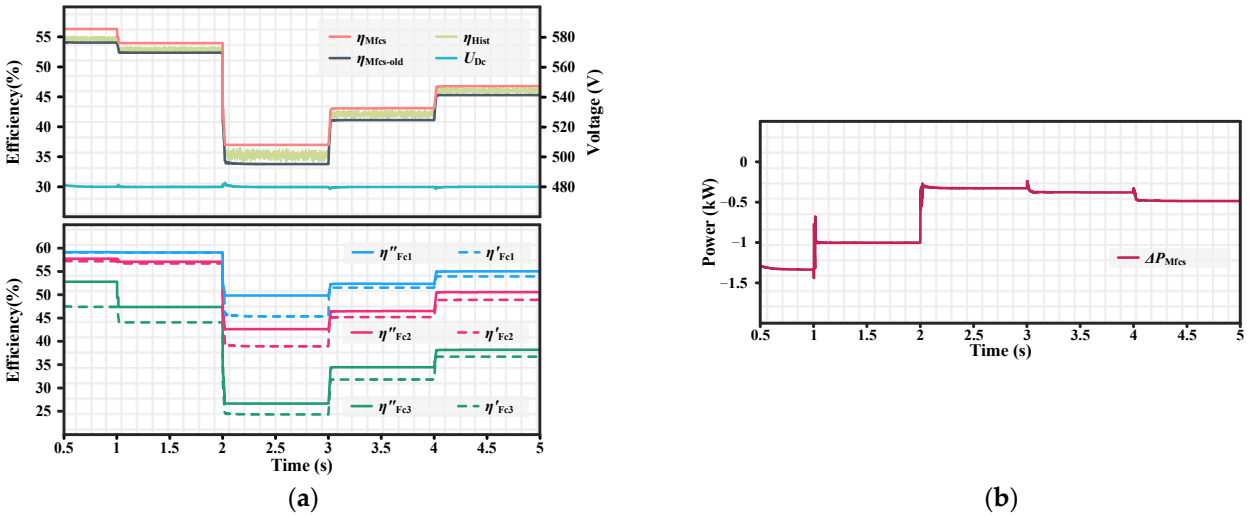


(**a**) (**b**)

**Figure 11.** Results of OP based on the ED power allocation strategy: (**a**) Efficiency of MFCS and $FC_i$ and bus voltage; (**b**) Power fluctuation of MFCS.

The interpretation of each parameter in Figure 11 is similar to that in Figure 10, except for the difference in the method used to solve the initial parameters. $P'_{\mathrm{fc}i}$ in Figure 10 comes from the FLC power allocation strategy, and $P'_{\mathrm{Fc}i}$ in Figure 11 comes from the ED power allocation strategy.

From the operational results of 0–5 s, it can be seen that $\eta_{\mathrm{Mfcs}}$ was always the optimal value of $\eta_{\mathrm{Hist}}$ under various operating conditions. Compared with $\eta_{\mathrm{Mfcs\text{-}old}}$, it can also be seen that OP makes the MFCS achieve an efficiency improvement rate of 3.2–9.5%;

synchronously, the efficiency improvement rate of the $FC_i$ can reach up to 9.4%. In addition, the bus voltage fluctuation rate was less than 0.55% during the process of OP.

In summary, OP has a certain universality and can be adapted to various MFCS power allocation strategies. OP maintains the stability of the microgrid while improving the electricity–hydrogen conversion efficiency of the MFCS.

## 5. Experimental Verification

In order to test and verify whether the coordinated control strategy proposed in this paper is feasible in actual working conditions, this section creates a virtual real-time scenario to simulate the microgrid operating environment of the HESS. Considering that HESS-related equipment is expensive and potentially dangerous while in operation, this paper chose the hardware-in-loop (HIL) experimental form and designed a digital experimental platform, as shown in Figure 12, to facilitate the conduct of the experiment and the observation of the results.

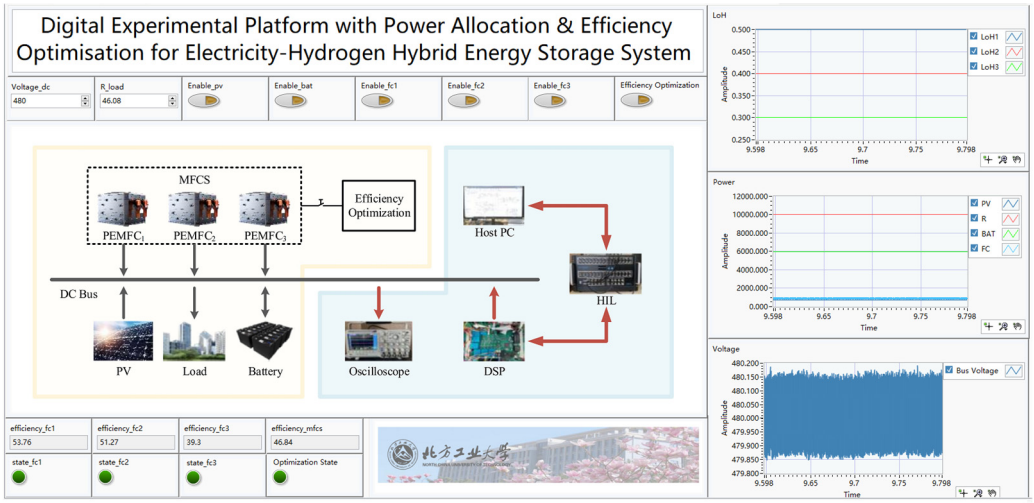


**Figure 12.** Digital experimental platform with power allocation and efficiency optimization for electricity-hydrogen hybrid energy storage system.

The initial values of $LoH_i$, $LoH_{\mathrm{mfcs}}$, and $SoC$ in the HIL simulation are shown in Table 7. In order to verify the application of the proposed strategy under variable working conditions, the photovoltaic power was increased from 0.8 kW to 8.5 kW under the premise that the load in the microgrid was constant at 10 kW.

**Table 7.** Initial parameters of the devices in the HIL experiment.

| $LoH_{\mathrm{fc1}}$ | $LoH_{\mathrm{fc2}}$ | $LoH_{\mathrm{fc3}}$ | $LoH_{\mathrm{mfcs}}$ | $SoC$ |
|---|---|---|---|---|
| 0.75 | 0.25 | 0.5 | 0.5 | 0.5 |

The application effect of the coordinated control strategy is shown in Figure 13. Except for a slight fluctuation in the bus voltage when the photovoltaic power suddenly increased, it stabilized at the rated value of 480 V at other times. During operation, the output power of the $FC_i$ was positively correlated with the $LoH_i$, and when $P_{\mathrm{net}}$ decreased from 9.2 kW to 2 kW, the power borne by $FC_i$ also decreased synchronously, and the overall output of the MFCS decreased from 5.2 kW to 0.83 kW. The experiment's results show that the proposed collaborative control strategy could adaptively compensate for the fluctuating $P_{\mathrm{net}}$ based on the margin of the energy storage device so that the bus voltage fluctuation rate was lower than 2.1% and maintained at a stable value.

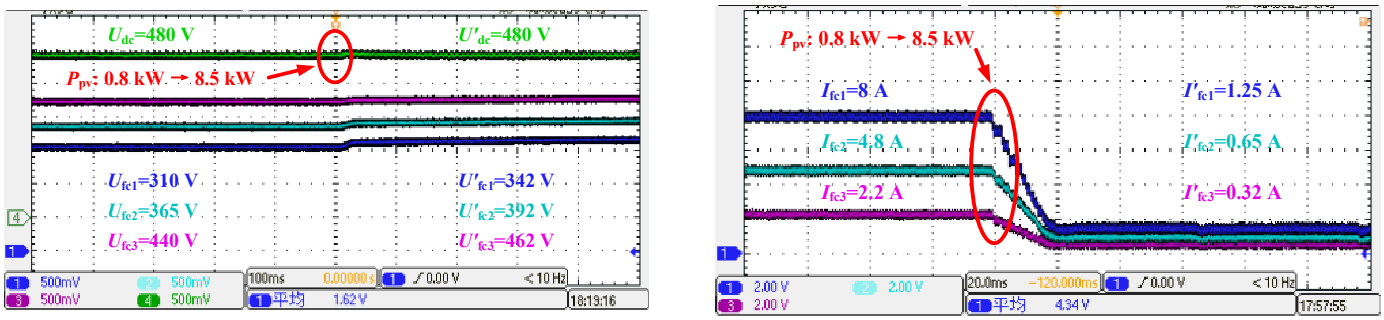


(**a**) (**b**)

**Figure 13.** Results of the HIL experiment: (**a**) Voltage of $FC_i$ and bus; (**b**) Current of $FC_i$.

## 6. Conclusions

This paper takes the HESS, composed of the MFCS and BESS in a DC microgrid, as the research object and proposes a coordinated control strategy for the efficiency improvement if the MFCS. After simulation and experimental verification of the proposed strategy, the following conclusions were obtained:

(1) The proposed upper system-level coordinated control strategy can realize the adaptive power allocation of the HESS using FLC according to the energy storage margin of the MFCS and BESS so that the energy storage system with a high energy storage margin can bear most of the fluctuating net power of the microgrid.

(2) The proposed lower device-level coordinated control strategy can further divide the overall power of the MFCS into single stacks according to the energy storage margin of the $FC_i$ using FLC so that the power borne by the $FC_i$ is positively correlated with $LoH_i$. The high, medium, and low ranges of the $LoH_i$ also correspond to the faster, moderate, and slower discharge rates of the $FC_i$.

(3) The proposed OP takes the power-efficiency characteristic of the FC as the starting point. After comprehensively considering the efficiency improvement in the MFCS, the output fluctuation rate of the MFCS, and the upper and lower limits of the energy storage system output, the power allocation of the $FC_i$ is adjusted in a perturbation manner based on the initial power allocation so that the efficiency improvement rate of the MFCS can reach up to 9.5%, and the efficiency improvement rate of the $FC_i$ can reach up to 8.6%.

(4) When sudden changes occur in the power of the photovoltaic or load power, the proposed coordinated control strategy can adaptively allocate and adjust the output power of the MFCS, BESS, and $FC_i$ so that the bus voltage can return to the steady-state value after experiencing a slight instantaneous fluctuation, with a fluctuation rate of less than 2.1%.

**Author Contributions:** Conceptualization, J.L., C.L., and Z.S.; methodology, C.L.; software, C.L.; validation, C.L. and Z.S.; formal analysis, C.L.; investigation, Z.S.; resources, J.L. and C.L.; data curation, C.L.; writing—original draft preparation, C.L.; writing—review and editing, C.L.; visualization, J.L. and Z.S.; supervision, J.L.; project administration, J.L. and Z.S.; funding acquisition, J.L. All authors have read and agreed to the published version of the manuscript.

**Funding:** This research was funded by the National Natural Science Foundation of China, grant number: 52277211, and Organized Research 2-Beijing Future Electrochemical Energy Storage System Integrated Technology Innovation Center, grant number: 110051360024XN149-11.

**Data Availability Statement:** Data will be made available upon request.

**Conflicts of Interest:** The authors declare no conflicts of interest.

## References


1. Alharbi, G.; Olabi, A.; Rezk, H.; Fathy, A.; Abdelkareem, M.A. Optimized energy management and control strategy of photovoltaic/PEM fuel cell/batteries/supercapacitors DC microgrid system. *Energy* **2024**, *290*, 130121. [CrossRef]
2. Zhang, Y.; Wei, W. Decentralised coordination control strategy of the PV generator, storage battery, and hydrogen production unit in islanded AC microgrid. *IET Renew. Power Gener.* **2020**, *14*, 1053–1062. [CrossRef]
3. Tan, C.; Tan, Q.; Geng, S.; Tan, Z.; Du, Y.; Xiao, J. Multi-timescale interaction of a coupled electricity-hydrogen-gas system with a distribution network considering dynamic games. *Sustain. Cities Soc.* **2023**, *96*, 104639. [CrossRef]
4. Hordé, T.; Achard, P.; Metkemeijer, R. PEMFC application for aviation: Experimental and numerical study of sensitivity to altitude. *Int. J. Hydrogen Energy* **2012**, *37*, 10818–10829. [CrossRef]
5. Sun, Y.; Shang, Q.; Jiang, W. Equivalent Minimum Hydrogen Consumption of Fuzzy Control-Based Fuel Cells: Exploration of Energy Management Strategies for Ships. *Batteries* **2024**, *10*, 66. [CrossRef]
6. Han, J.; Charpentier, J.; Tang, T. An Energy Management System of a Fuel Cell/Battery Hybrid Boat. *Energies* **2014**, *7*, 2799–2820. [CrossRef]
7. Hegazy, R.; Ahmed, F. Hydrogen reduction-based energy management strategy of hybrid fuel cell/PV/battery/supercapacitor renewable energy system. *J. Energy Storage* **2024**, *86*, 111316.
8. Ferahtia, S.; Djeroui, A.; Rezk, H.; Houari, A.; Zeghlache, S.; Machmoum, M. Optimal control and implementation of energy management strategy for a DC microgrid. *Energy* **2022**, *238*, 121777. [CrossRef]
9. Versaci, M.; Foresta, L. Fuzzy Approach for Managing Renewable Energy Flows for DC-Microgrid with Composite PV-WT Generators and Energy Storage System. *Energies* **2024**, *17*, 402. [CrossRef]
10. Mei, J.; Meng, X.; Tang, X.; Li, H. An Accurate Parameter Estimation Method of the Voltage Model for Proton Exchange Membrane Fuel Cells. *Energies* **2024**, *17*, 2917. [CrossRef]
11. Jiang, D.; Long, Y.; Fu, P.; Guo, C.; Tang, Y.; Huang, H. A novel multi-stack fuel cell hybrid system energy management strategy for improving the fuel cell durability of the hydrogen electric Multiple Units. *Int. J. Green Energy* **2024**, *21*, 1766–1775. [CrossRef]
12. Kamel, A.; Rezk, H.; Shehata, N.; Thomas, J. Energy Management of a DC Microgrid Composed of Photovoltaic/Fuel Cell/Battery/Supercapacitor Systems. *Batteries* **2019**, *5*, 63. [CrossRef]
13. Marx, N.; Boulon, L.; Gustin, F.; Hissel, D. A review of multi-stack and modular fuel cell systems: Interests, application areas and on-going research activities. *Int. J. Hydrogen Energy* **2014**, *39*, 12101–12111. [CrossRef]
14. Li, Y.; Zhao, X.; Liu, Z.; Li, Y.; Chen, W.; Li, Q. Experimental study on the voltage uniformity for dynamic loading of a PEM fuel cell stack. *Int. J. Hydrogen Energy* **2015**, *40*, 7361–7369. [CrossRef]
15. Yan, X.; Hou, M.; Sun, L.; Cheng, H.; Youlu, H.; Liang, D.; Shen, Q.; Ming, P.; Yi, B. The study on transient characteristic of proton exchange membrane fuel cell stack during dynamic loading. *J. Power Sources* **2006**, *163*, 966–970. [CrossRef]
16. Wang, T.; Li, Q.; Yang, H.; Yin, L.; Wang, X.; Qiu, Y.; Chen, W. Adaptive current distribution method for parallel-connected PEMFC generation system considering performance consistency. *Energy Convers. Manag.* **2019**, *196*, 866–877. [CrossRef]
17. Tang, X.; Shi, L.; Zhang, Y.; Li, B. Degradation adaptive energy management strategy for FCHEV based on the Rule-DDPG method: Tailored to the current SOH of the powertrain. *IEEE Trans. Transp. Electrif.* **2024**. [CrossRef]
18. Wang, Y.; Chen, W.; Li, Q.; Han, Y.; Guo, A.; Wang, T. Coordinated optimal power distribution strategy based on maximum efficiency range of multi-stack fuel cell system for high altitude. *Int. J. Hydrogen Energy* **2024**, *50*, 374–387. [CrossRef]
19. Suresh, R.; Sankaran, G.; Joopudi, S.; Choudhury, S.R.; Narasimhan, S.; Rengaswamy, R. Optimal power distribution control for a network of fuel cell stacks. *J. Process Control* **2019**, *74*, 88–98. [CrossRef]
20. Garcia, F.; Herrera, D.; Boulon, L.; Sicard, P.; Hernandez, A. Power sharing for efficiency optimisation into a multi fuel cell system. In Proceedings of the International Symposium on Industrial Electronics (ISIE), Istanbul, Turkey, 1–4 June 2014; pp. 218–223.
21. Wang, T.; Li, Q.; Yin, L.; Chen, W.; Breaz, E.; Gao, F. Hierarchical power allocation method based on online extremum seeking algorithm for dual-PEMFC/battery hybrid locomotive. *IEEE Trans. Veh. Technol.* **2021**, *70*, 5679–5692. [CrossRef]
22. Li, Q.; Liu, Q.; Wang, T.; Chen, W. Maximum efficiency point tracking control method of multi-stack fuel cell system based on EKF online identification. *Proc. CSEE* **2022**, *42*, 673–684.
23. Liu, Q.; Li, Q.; Wang, T.; Cai, L.; Chen, W. Efficiency Optimal Control Method of Multi-stack Fuel Cell System Based on Salp Swarm Algorithm. *Proc. CSEE* **2021**, *41*, 7730–7740.
24. Yang, M.; Li, Q.; Cai, L.; Wang, T.; Chen, W. Multi-objective Optimization Energy Management Method for Fuel Cell Hybrid Power System Considering Stack Performance Consistency. *Proc. CSEE* **2024**, *44*, 385–395.
25. Yilmaz, M. Comparative Analysis of Hybrid Maximum Power Point Tracking Algorithms Using Voltage Scanning and Perturb and Observe Methods for Photovoltaic Systems under Partial Shading Conditions. *Sustainability* **2024**, *16*, 4199. [CrossRef]
26. Awad, M.; Ibrahim, A.; Alaas, Z.; El-Shahat, A.; Omar, A.I. Design and analysis of an efficient photovoltaic energy-powered electric vehicle charging station using perturb and observe MPPT algorithm. *Front. Energy Res.* **2022**, *10*. [CrossRef]
27. Chen, J.; He, H.; Quan, S.; Wei, Z.; Zhang, Z.; Wang, Y.-X. Real-time power optimization based on PSO feedforward and perturbation & observation of fuel cell system for high altitude. *Fuel* **2024**, *356*, 129551.
28. Peña, J.; Rodríguez, C.; Avalos, G. Study of a New Wave Energy Converter with Perturb and Observe Maximum Power Point Tracking Method. *Sustainability* **2023**, *15*, 10447. [CrossRef]

29. Ozpineci, B.; Du, Z.; Tolbert, L.M.; Adams, D.J.; Collins, D. Collins Integrating multiple solid oxide fuel cell modules. In Proceedings of the IECON'03, 29th Annual Conference of the IEEE Industrial Electronics Society, Roanoke, VA, USA, 2–6 November 2003; Volume 2, pp. 1568–1573.
30. Long, R.; Yin, Z.; Zhang, L.; Chen, Q.; Quan, S. Design of power allocation strategy and passivity based controller for multiple module fuel cell hybrid power system. In Proceedings of the 2017 29th Chinese Control and Decision Conference (CCDC), Chongqing, China, 28–30 May 2017; pp. 4944–4948.
31. Chen, W.; Zhu, Y.; Li, Q.; Deng, H.; Hong, Z. Review and Prospect of Structures, Control and Detection Schemes of Multi-stack Fuel Cell Power Generation System Used in Rail Traffic. *Proc. CSEE* **2018**, *38*, 6967–6980.
32. He, D.; Zhang, W.; Luo, X. Overview of Power Lithium Battery Modeling and Soc Estimation. In Proceedings of the International Conference on Energy Equipment Science and Engineering (IOP), Harbin, China, 29 November–1 December 2019; Volume 461, p. 012032.
33. Zhang, R.; Li, X.; Sun, C.; Yang, S.; Tian, Y.; Tian, J. State of Charge and Temperature Joint Estimation Based on Ultrasonic Reflection Waves for Lithium-Ion Battery Applications. *Batteries* **2023**, *9*, 335. [CrossRef]
34. Wang, Y.; Yang, X.; Sun, Z.; Chen, Z. A systematic review of system modeling and control strategy of proton exchange membrane fuel cell. *Energy Rev.* **2024**, *3*, 100054. [CrossRef]
35. Tang, X.; Yang, M.; Shi, L.; Hou, Z.; Xu, S.; Sun, C. Adaptive state-of-health temperature sensitivity characteristics for durability improvement of PEM fuel cells. *Chem. Eng. J.* **2024**, *491*, 151951. [CrossRef]
36. Hong, Z.; Li, Q.; Han, Y.; Shang, W.; Zhu, Y.; Chen, W. An energy management strategy based on dynamic power factor for fuel cell/battery hybrid locomotive. *Int. J. Hydrogen Energy* **2018**, *43*, 3261–3272. [CrossRef]
37. Wang, X.; Guo, Q.; Tu, C.; Che, L.; Hou, Y.; Xiao, F. A two-layer control strategy for hydrogen-battery hybrid system considering the efficiency characteristics of MS-PEMFC. *Electr. Power Syst. Res.* **2023**, *225*, 109818. [CrossRef]
38. Rodriguez, R.; Trovão, J.; Solano, J. Fuzzy logic-model predictive control energy management strategy for a dual-mode locomotive. *Energy Convers. Manag.* **2022**, *253*, 115111. [CrossRef]
39. Lin, X.; Xi, L.; Wang, Z. Battery degradation-aware energy management strategy with driving pattern severity factor feedback correction algorithm. *J. Clean. Prod.* **2024**, *45*, 141969. [CrossRef]